

Characterization, Thermodynamics and Mechanism of Formation of SiC-SiO_x Core–Shell Nanowires



ANDREA BROGGI, ELI RINGDALEN, and MERETE TANGSTAD

Silicon carbide nanowires are valuable for electronic and optical applications, due to their high mechanical and electrical properties. Previous studies demonstrated that nanowires can be produced easily, by mixing a silicon-based compound (Si or SiO₂) with a carbon source (C or SiC), in an inert gas atmosphere (Ar or He). The result of this reaction is an elevated number of core–shell SiC-SiO_x nanowires. The mechanism of formation of these wires should be inquired, in order to control the process. In this work, SiO₂ and SiC are chosen as raw materials for SiO(g) and CO(g) production. These two gases react at SiC surfaces and generate the core–shell nanowires. SEM, TEM and XPS analyses confirm the composition and the microstructure of the product. A three-step mechanism of formation is proposed. The formation of nanowires is compared with thermodynamics of reactions occurring in the Si-C-O system. It is found that nanowires develop in wide temperature and SiO partial pressure ranges (T: 924 °C to 1750 °C, $p_{\text{SiO}} = 0.50$ to 0.74). Higher He flows will shift the reaction to lower temperatures and p_{SiO} .

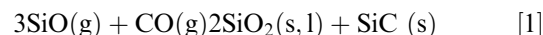
<https://doi.org/10.1007/s11663-020-02014-4>
© The Author(s) 2020

I. INTRODUCTION

SILICON carbide has been heavily investigated in the recent years, due to its high thermal, electrical and mechanical properties. Some of these properties are preserved also in extreme conditions, for example in the thermal protection applications. SiC is used also as semiconductor material for transistors and sensors. Applications of SiC nanomaterials range from reinforcements in epoxydic materials to light-emitting devices.^[1,2]

SiC nanostructured materials can be produced in a wide range of temperature and gas composition. Most of the studies are performed at atmospheric pressure, utilizing a simple production method.^[3–20] The procedure is always based on the same principle. A mixture of raw materials (Si or SiO₂, C or SiC, Ar) is heated, until it produces a gas phase, consisting mainly of SiO(g) and CO(g). The gas mixture will react once it reaches a lower temperature substrate. Reaction (1) will be the nanowire production reaction from the gas phase. In this case, core–shell SiC-SiO_x nanowires would form without requiring any added catalyst to the system. These

materials can either be used for electronic application as they are or treated with leaching to remove the oxide shell. Small overpressures to 1.5 atm do affect microstructure.^[21]



Different synthesis approaches may influence the formation mechanism of SiC nanowires, and consequently their final microstructure and composition. There are many theories concerning the mechanism of formation of SiC nanowires. The most common are vapor–solid growth, vapor–liquid–solid growth^[22,23] and oxide-assisted growth (OAG).^[11,12,24,25] The OAG mechanism explains the formation of the core–shell nanowires, with oxides on the shell phase. The partial pressure of SiO(g) in the gas phase (p_{SiO}) is believed to be the driving force for Reaction (1), which undergoes out of equilibrium conditions.^[4,9,26–30]

Broggi *et al.*^[28] study the thermodynamics for another reaction, which occurs simultaneously with Reaction (1) and produces a Si-SiO₂ mixture from SiO(g) and CO(g). First, a mass balance is assessed between the SiO-CO gas mixture produced and the products collected, which are the SiC-SiO_x nanowires and the Si-SiO₂ mixture. p_{SiO} in the gas is calculated before and after the two reactions occurred. Then, the temperature and the position of the products in the crucible are related by measuring the temperature gradient in the setup. Finally, p_{SiO} is related to temperature by locating where condensation started and ended in the crucible.

ANDREA BROGGI and MERETE TANGSTAD are with the University of Science and Technology (NTNU), Department of Materials Science and Engineering, Alfred Getz vei 2b, 7034 Trondheim, Norway. Contact e-mail: andrbrog@ntnu.no ELI RINGDALEN is with the SINTEF, Alfred Getz vei 2b, 7034 Trondheim, Norway.

Manuscript submitted May 20, 2020; accepted October 16, 2020.

The aim of this paper is to use the mass balance, temperature measurements and p_{SiO} calculations of the experiments by Broggi *et al.*,^[28] to discuss the thermodynamics of Reaction (1). This work is complementary to Broggi *et al.*,^[28] whose aim was to discuss the thermodynamics of the Si-SiO₂ mixture formation. Relevant earlier results are also reported. The paper discusses the effect of gas composition on the amount of nanowires and on their temperature of formation. In the end, a dedicated OAG mechanism is described for SiC-SiO_x core-shell nanowires. The mechanism is based on SEM and TEM characterization of nanowires and comparison with previous works from literature.

II. EXPERIMENTAL SECTION

All the information about raw materials characterization, pellets preparation, temperature measurements, furnace operation, sample preparation and characterization are described by Broggi *et al.*^[28] At the bottom of the graphite tube furnace there is a gas production chamber, which gives SiO(g) and CO(g) from SiC and quartz pellets. The gas ascends, pushed by He(g) or Ar(g), and produces nanowires on the SiC particles in the reaction chamber. The reaction chamber has a vertical temperature gradient, measured either by a triple-point thermocouple, or by a single-point thermocouple placed at different positions during each experiment repetition. The experimental setup is drawn in Figure 1.

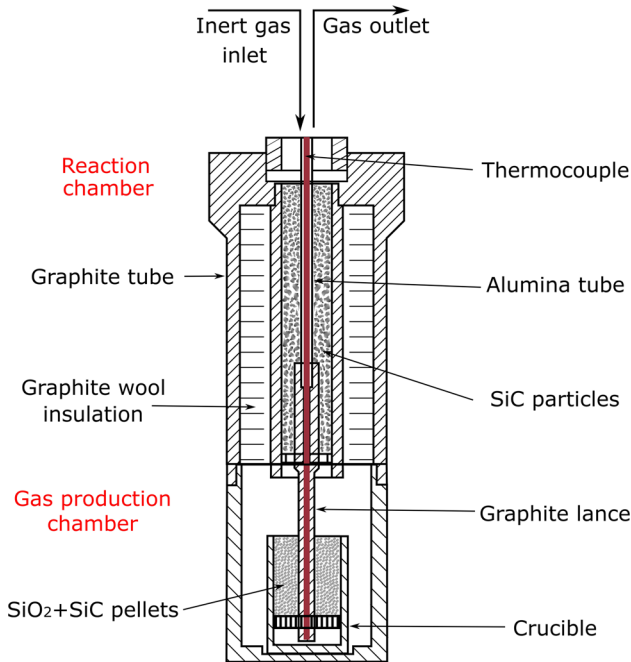


Fig. 1—Schematic overview of the graphite tube furnace setup. Reprinted with permission^[28] 2019, Met. Mater. Trans B.

The injected gas flow and holding time were varied between each series (Table I). A new experiment was added (Experiment 2a in this work), compared to Broggi *et al.*^[28] The series are marked with a number from 1 to 7, and by a letter from *a* to *e*, defining the repetition of each series.

TEM samples were analyzed with the same microscope as Broggi *et al.*,^[28] but collected in a different way. Samples were scratched from the SiC particles. The scratched crumbs were mixed with isopropanol. A droplet of the solution was extracted and placed on a copper TEM grid. After drying overnight at 120 °C, the sample was ready for analysis.

III. RESULTS

After every experiment, the majority of the SiC particles in the reaction chamber were covered into two different kind of layers, called, respectively, blue and white condensate. The layers can be easily removed by scratching the SiC substrates. When scratching white condensate, blue condensate often appears. Both blue and white layers appear as a disordered web of nanowires (Figures 2 and 3). Some of the nanowires

Table I. Experimental Conditions: Holding Times at 2000 °C (2273 K) and Gas Flows

Series	Time [h]	Gas flow [l min ⁻¹]
1 (a) to (e)	1	0.40 <i>a</i> = Ar <i>b-e</i> = He
2 (a)	0.5	0.10, He
3 (a)	1	0.10, He
4 (a)	1	0.05, Ar
5 (a)	0.5	0.02, Ar
6 (a) to (e)	1	0.02, Ar
7 (a)	4	0.02, Ar

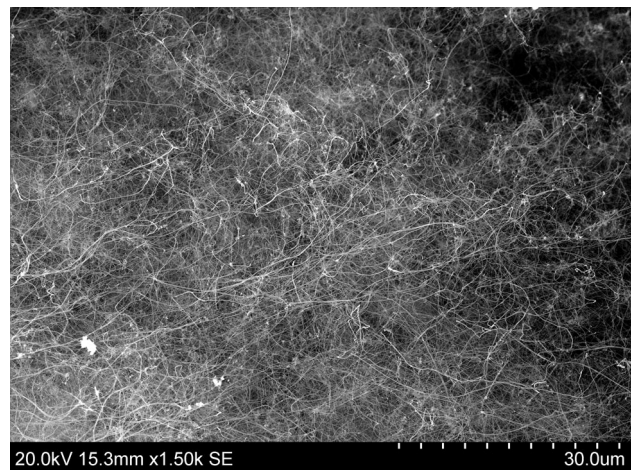


Fig. 2—Blue condensate from Experiment 4a, 1150 °C to 1250 °C. Reprinted from Ref. [21] under the terms of the Creative Commons CC BY 4.0 license.”.

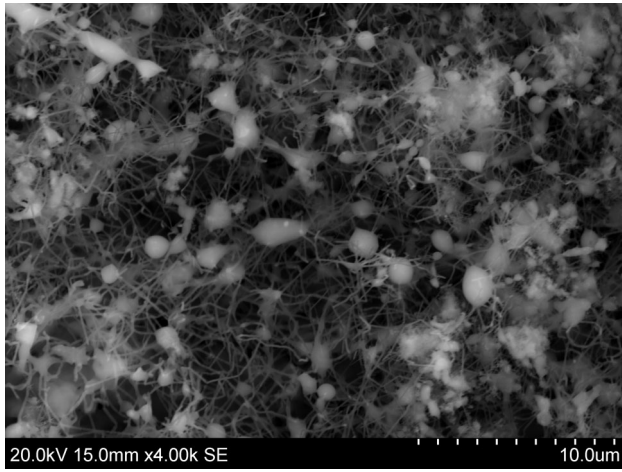


Fig. 3—White condensate from Experiment 5a, $T = 1150\text{ }^{\circ}\text{C}$ to $1750\text{ }^{\circ}\text{C}$.

are embedded in nodules, especially where the nanowires are close. The size of the nodules ranges between 0.25 and $1.0\text{ }\mu\text{m}$. There are more nodules in the white condensate than in the blue.

The blue condensate appears both at the top and at the bottom of the condensation chamber, in the temperature ranges $900\text{ }^{\circ}\text{C}$ to $1250\text{ }^{\circ}\text{C}$ and $1610\text{ }^{\circ}\text{C}$ to $1800\text{ }^{\circ}\text{C}$. The white condensate generates between $1150\text{ }^{\circ}\text{C}$ and $1780\text{ }^{\circ}\text{C}$ (Figure 3). The nanowire production starts from the highest temperatures, and propagates upwards in the condensation chamber, toward lower temperatures.

A. TEM Analysis

1. Blue condensate

Blue condensate was collected for topographic and compositional analysis. A sample was extracted in the position zones corresponding to $1180\text{ }^{\circ}\text{C}$ to $1500\text{ }^{\circ}\text{C}$ from Experiment 6c. The wires exhibit a core-shell structure. The core and shell sizes are marked on Figure 4. The shell can coat many wires at the same time. The core size ranges around 10 to 20 nm in diameter, and the external layer can give a nanowire size up to 70 to 80 nm width. The nodule diameter can reach up to 200 nm .

Figure 5 shows Electron Dispersive X-ray Spectroscopy-Electron Energy Loss Spectroscopy (EDX-EELS) line compositional scanning of a single wire in the proximity of its tip. Si concentration increases when going toward the core. The same happens to C, whereas O follows the opposite trend. Stacking faults in the core phase can be noticed from Figure 6. The plane spacing was measured to be between 2.2 and 2.5 \AA , which corresponds to the results from Hu *et al.*^[11,12] The composition of the core phase is 3C-SiC , even if the lateral side of the core phase is not perfectly crystalline. The shell phase, containing oxygen and silicon, can be identified as SiO_x . The shell phase did not show any preferential crystallographic orientation.

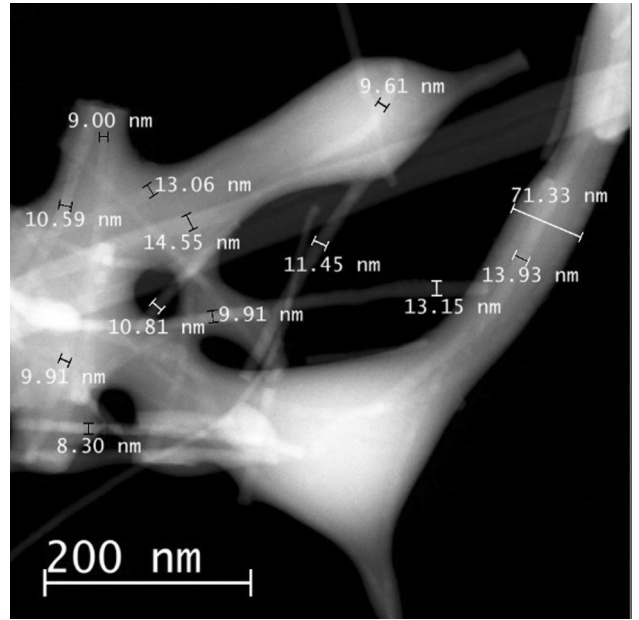


Fig. 4—Dimension of core and shells in nanowires of blue condensate.

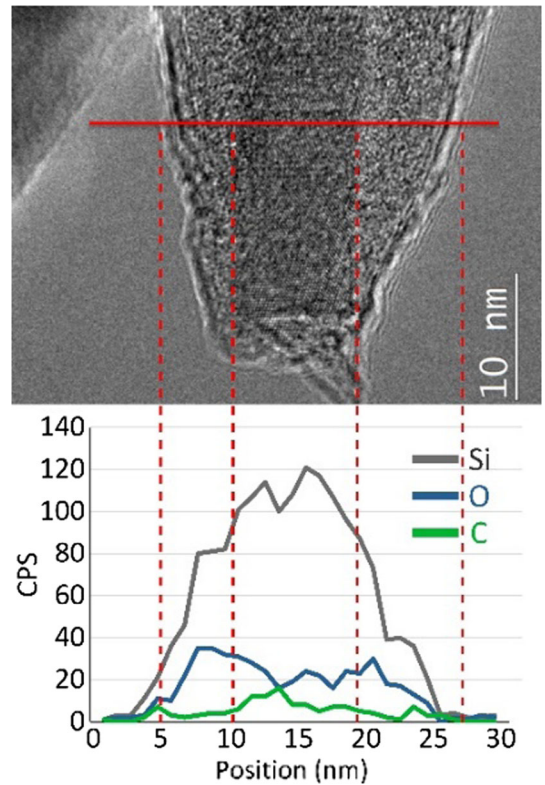


Fig. 5—Line scanning of blue condensate nanowire tip. Elemental analysis of silicon (gray), oxygen (blue) and carbon (green) in counts per second.

2. White condensate

Figures 7 and 8 show the typical features of white condensate. First, the nanowires have similar thicknesses with respect to the blue condensate. The nodules are placed periodically on the surface, as pearls on a necklace. Some of the wires (or some portions of them) are not covered by the SiO_x shell phase. Stacking faults form in the core phase (Figure 7) regardless from the microstructure of the shell phase.^[21] Figure 8a and b takes also a closer look at the interface between the core and the shell phase. SiO_x nodules can stick to more than a SiC nanowire at the same time (Figure 8a). The shell

phase has a curved surface (Figure 8b). A well-defined interface is present between the SiC core and the amorphous SiO_x nodules.

EDX elemental mapping was taken in proximity of a nodule, to verify the core and the shell compositions (Figure 9). A portion of a wire is not covered by the shell phase, on the right side of the picture. On the right side, the nanowire is visible both in the Si and C mapping. O and Si are present in the nodule. To summarize, the core phase is made of Si and C only, and the shell is made of Si and O.

B. XPS Analysis

Both the samples for XPS were extracted from Experiment 6c, in the temperature range $T = 1580\text{ }^\circ\text{C}$ to $1706\text{ }^\circ\text{C}$. Figure 10 shows the surfaces from which the spectra were collected. Sample 1 is a SiC particle covered in the blue condensate. Sample 2 is a scale detached from a SiC particle. Sample 2 has both blue and white color, therefore the analysis was carried out on each color zone (2.1 and 2.2 in Figure 10).

Figures 11, 12, and 13 show the XPS spectra collected for the three inquired points. All the spectra present four well-defined peak groups. Peaks in the 530 eV area are coming from O-1s electrons. C-1s electrons are revealed at 280 eV, whereas Si-2s and Si-2p are revealed at 150 and 100 eV, respectively. The atomic composition calculated from the survey spectra are close to the expected composition, *i.e.*, a $\text{SiO}_2:\text{SiC} = 2:1$ molar ratio mixture. This mixture consists of 37.5 at. pct Si, 50.0 at. pct O and 12.5 at. pct C.

Each peak group will describe how the electrons of different atoms from different orbitals would interact. The O-1s and Si-2s electrons give a single characteristic peak, respectively, at 532.5 and 152 eV (Figure 14). Si-2s and O-1s electrons are involved in Si=O bonds, which would occur in silica. This happens for every sample analyzed.

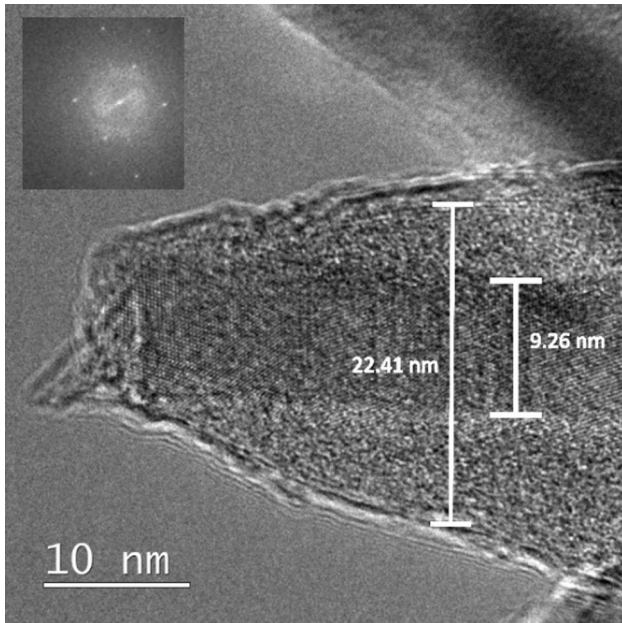


Fig. 6—Zoom on a nanowire tip and diffraction pattern of the picture. Stacking faults between atomic planes can be seen in the core phase. Reprinted from Ref. [21] under the terms of the Creative Commons CC BY 4.0 license.”.

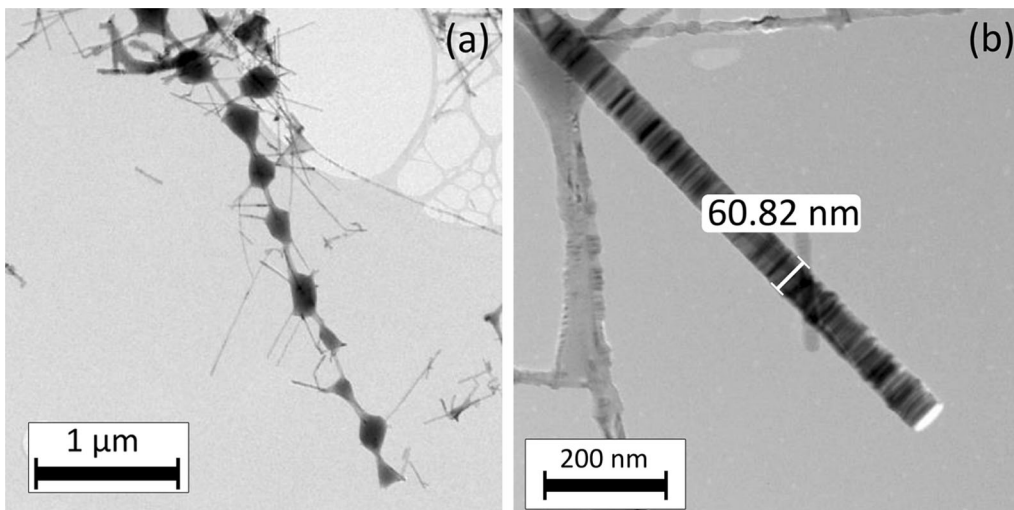


Fig. 7—Nanowires from Experiment 6c, $T = 1500\text{ }^\circ\text{C}$ to $1580\text{ }^\circ\text{C}$. (a) Bead structure; (b) Stacking faults in SiC nanowire. Reprinted from Ref. [21] under the terms of the Creative Commons CC BY 4.0 license.”.

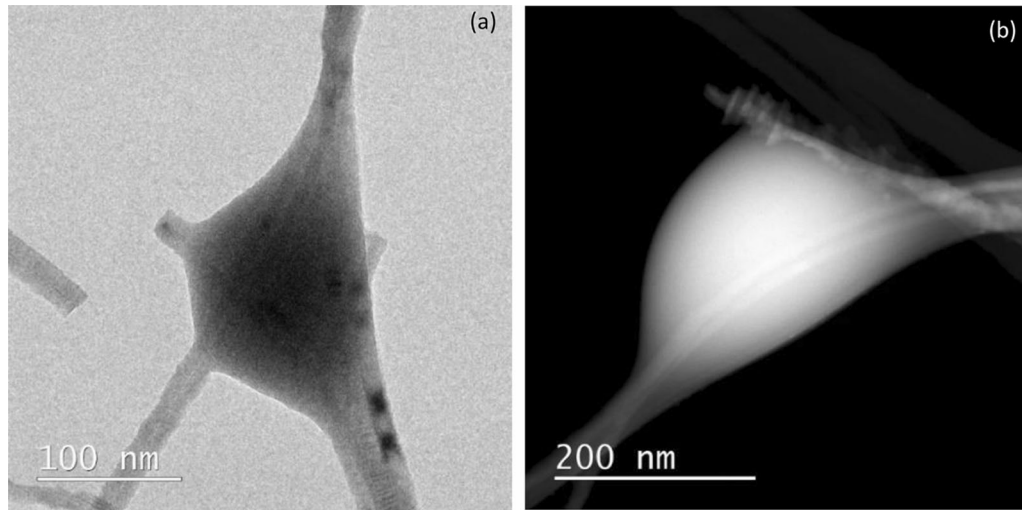


Fig. 8—Nodules, shell and core phases of SiC-SiO_x nanowires. Experiment 6c, $T = 1500\text{ }^{\circ}\text{C}$ to $1580\text{ }^{\circ}\text{C}$; (a) Image obtained by Selected Area Diffraction Analysis in Bright Field (SADA-BF). (b) Image obtained by High Angle Annular Dark Field Scanning Transmission Electron Microscopy (HAADF-STEM).

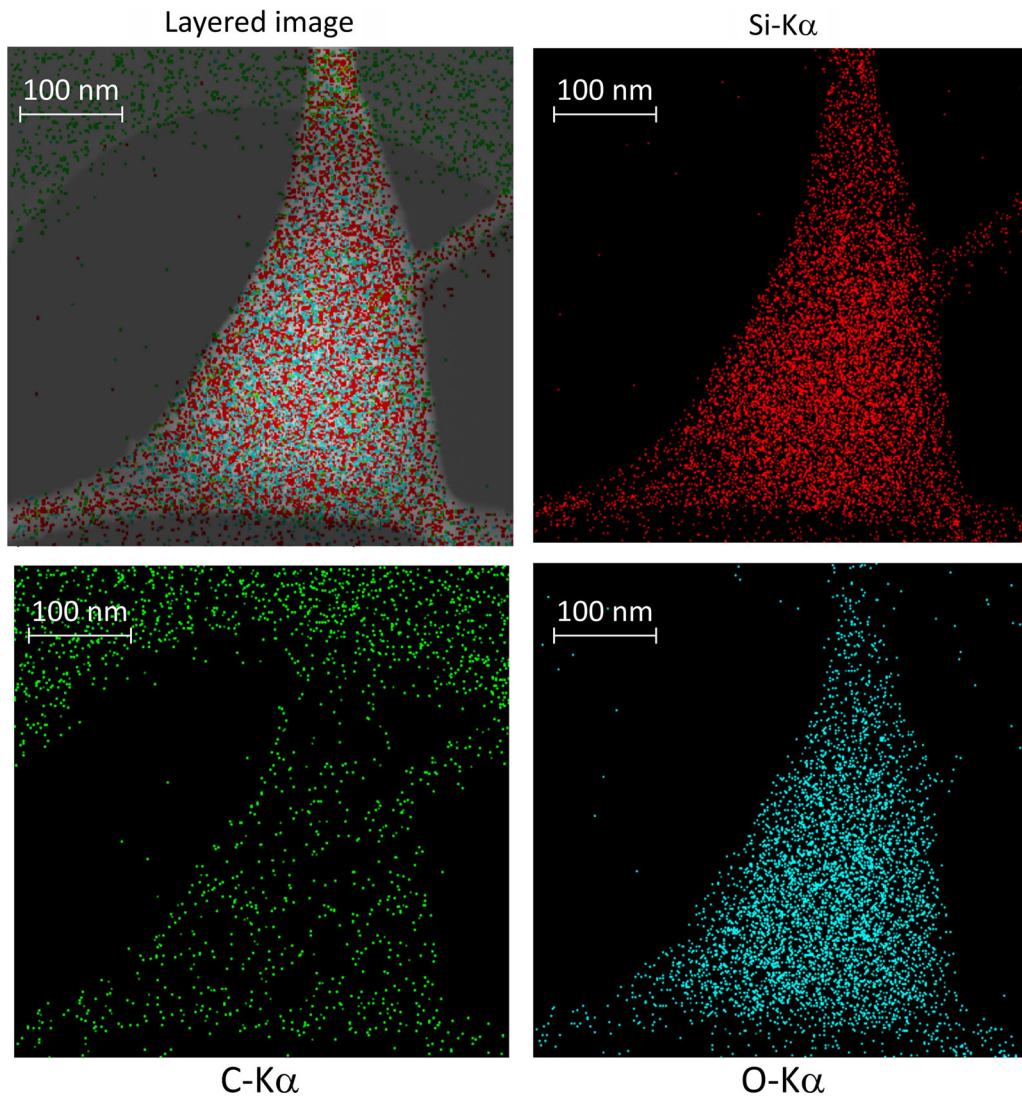


Fig. 9—EDS mapping of Si (red), C (green) and O (light blue) of a nodule and incoming wire, from TEM analysis of white condensate. Sample from Experiment 6c, $T = 1500\text{ }^{\circ}\text{C}$ to $1580\text{ }^{\circ}\text{C}$.

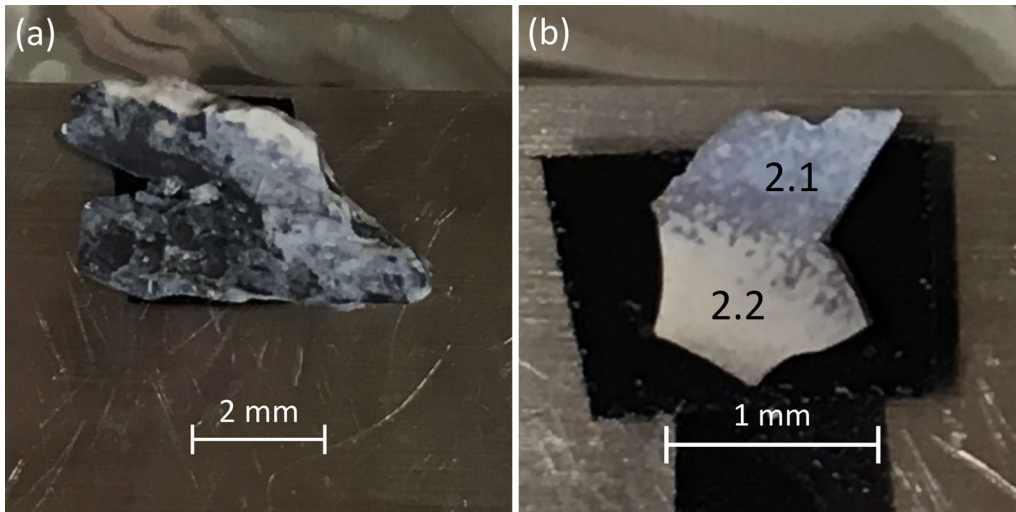


Fig. 10—(a) Sample 1; (b) Sample 2, positions of points 2.1 and 2.2.

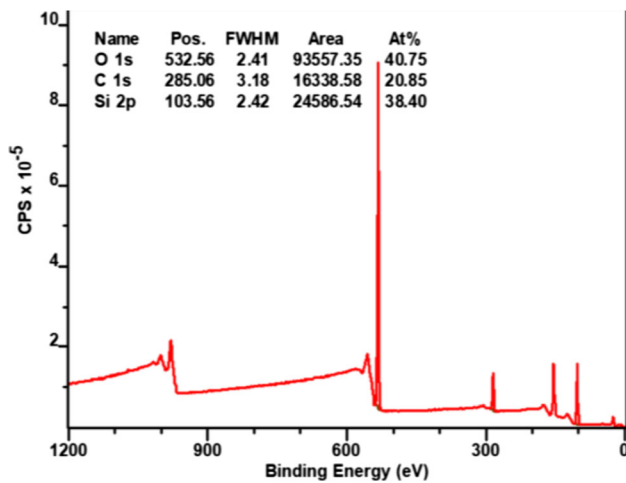


Fig. 11—Survey spectrum of sample 1, blue condensate.

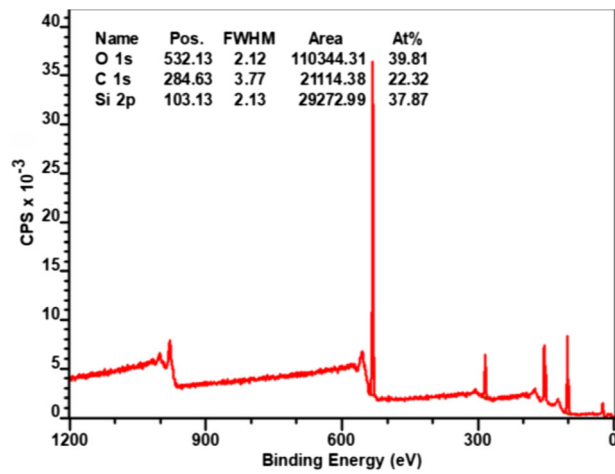


Fig. 13—Survey spectrum of point 2.2, white condensate.

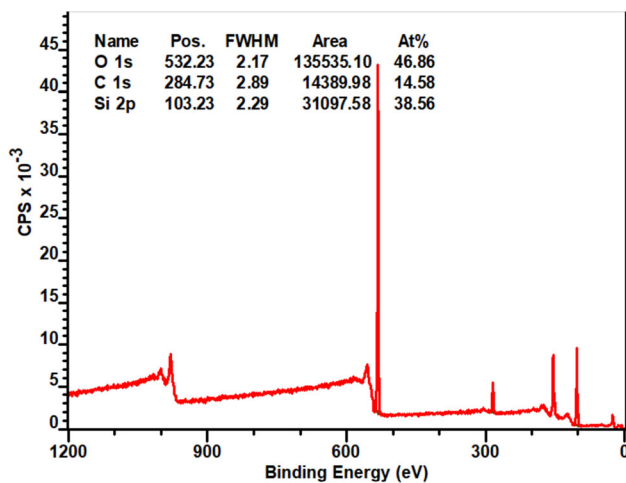


Fig. 12—Survey spectrum of point 2.1, blue condensate.

The electrons involved in Si-O, Si-Si and Si-C bonds belong to the Si-2p and C-1s groups. The spectra of these groups are shown in Figures 15, 16, and 17. The Si-2p spectrum shows only two major peaks. The first is located at 103.5 eV (Si-O), and the second between 100 and 101 eV (Si-Si). The second peak often splits into two peaks, as the Si-C and Si-Si peak overlap. In the C-1s group, the most present bonds are C-C and Si-C (carbide). Other minor peaks such as C-O-C, C=O, C-OH and C-O=C were detected. They are usually associated to organic impurities on the surface. The carbide signal in the C-1s sub-spectrum is relatively strong (35.72 at. pct).

Since the substrate particle is also made of SiC, the C-1s peaks could receive some signal from the substrate as well. However, the X-rays penetrate down to a few nm. The wires are entangled in a thick web, with small free spaces between them. Only small part of the XPS

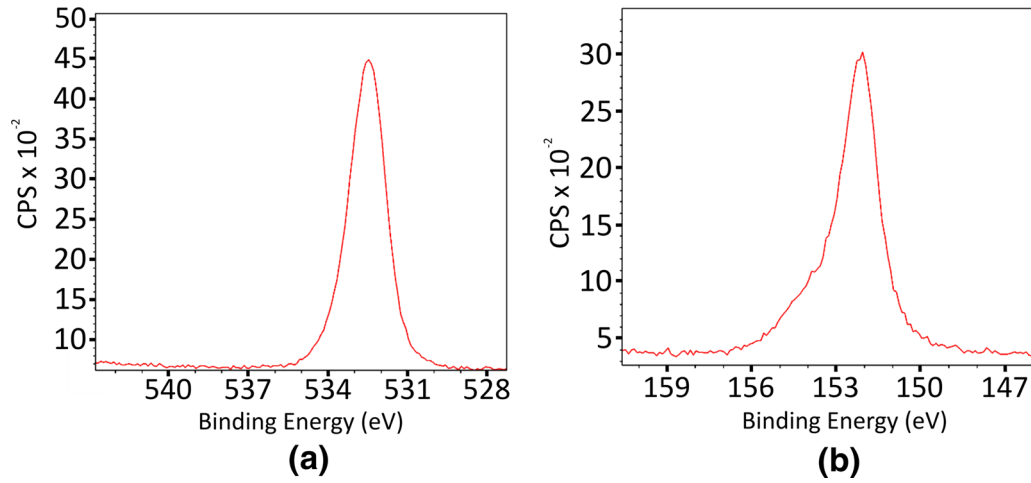


Fig. 14—(a) O-1s electron XPS spectrum; (b) Si-2s electron XPS spectrum, sample 2.1.

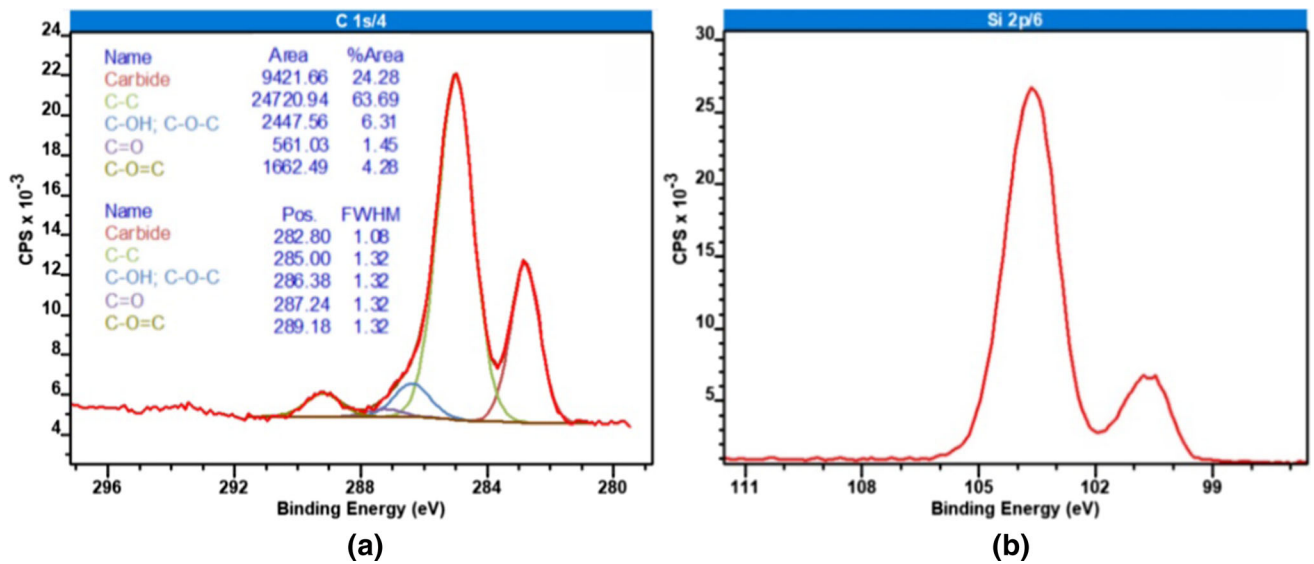


Fig. 15—(a) C-1s electron XPS spectrum, (b) Si-2p electrons XPS spectrum. Sample 1, blue condensate.

detected signal would come from the substrate, as it will encounter many obstacles on its way toward the substrate surface.

IV. DISCUSSION

A. Partial Pressure and Temperature of Formation

The nanowires produced with this process look very similar to the core-shell nanowires produced in previous works.^[3–20] The difference lies in the raw materials chosen for the gas production. Carbon was used in many previous works,^[7,11–15,20] instead of SiC. Commercial carbon powders are preferred since they are cheaper and easily available, compared to SiC. Despite that, the gas production reactions would be the same. In

fact, SiO₂ can react with C through Reaction (2). Once SiC is generated, Reaction (3) would take place in the pellets crucible, above 1450 °C.^[31,32] In other words, Reaction (2) can be “bypassed” by mixing SiO₂ and SiC in the pellets.



Silicon carbide and silicon were found on the graphite walls of the gas production zone, thanks to Reactions (4 through 6).^[33] The reactions might be a cause of reduction of SiO(g) content in the system, making p_{SiO} lower than expected.

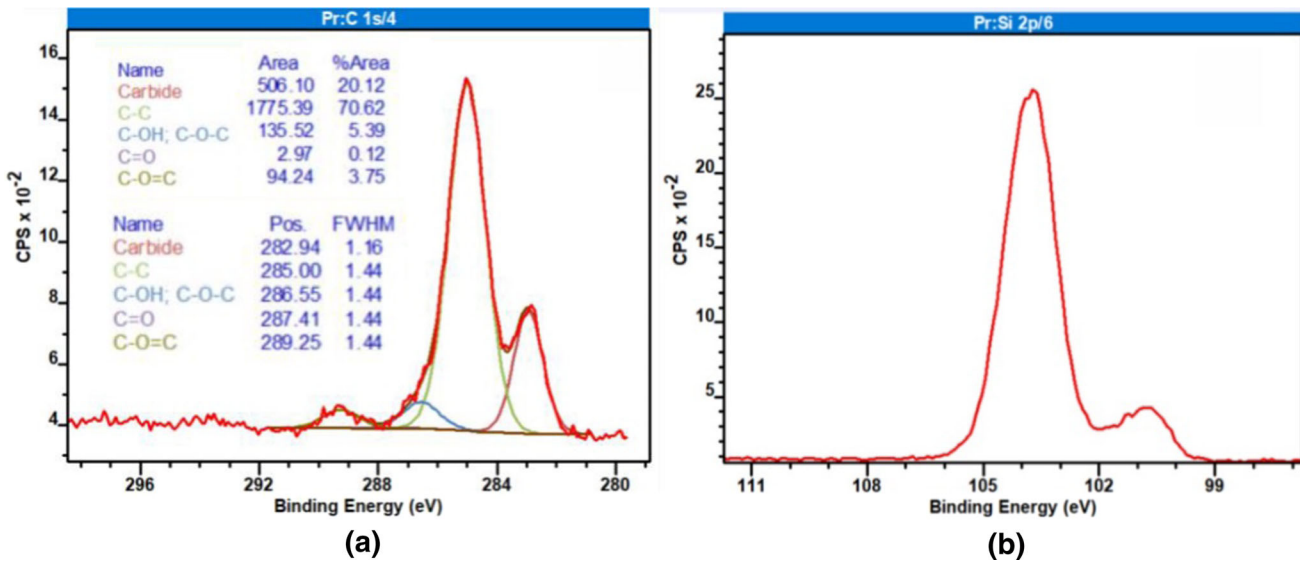


Fig. 16—(a) C-1s electron XPS spectrum, (b) Si-2p electrons XPS spectrum. Sample 2.1, blue condensate.

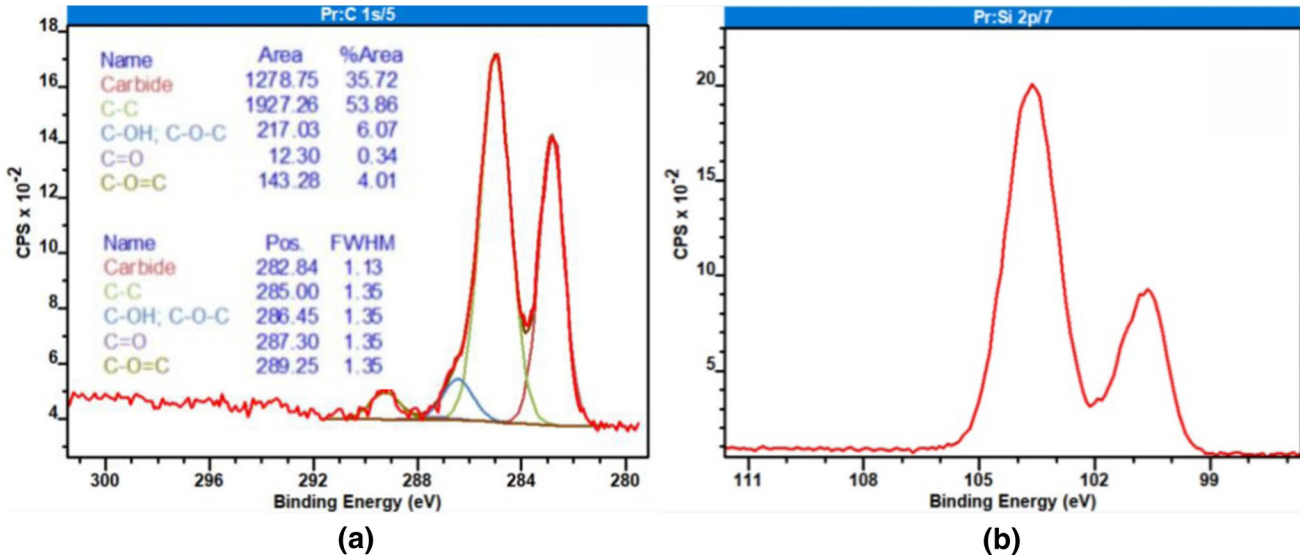
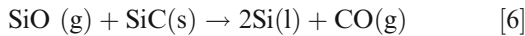


Fig. 17—(a) C-1s electron XPS spectrum, (b) Si-2p electrons XPS spectrum. Sample 2.2, white condensate.



The partial pressure and temperature of formation concepts of $T_{\text{SiO,in}}$, $p_{\text{SiO,in}}$, $T_{\text{SiO,R1,start}}$, $p_{\text{SiO,R1,start}}$, $T_{\text{SiO,out}}$ and $p_{\text{SiO,out}}$ are the same as in Broggi *et al.*^[28] However, in this work the notation *R1* refers to nanowires formation, and not to the Si-SiO₂ mixture production. The Si-SiO₂ mixture production from SiO(g) will be called Reaction (7).

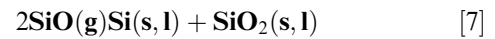


Table II collects all the temperature and pressure parameters, together with the amounts of Si-SiO₂ mixture and SiC-SiO_x nanowires, for each experiment. The amount of SiC-SiO_x nanowire tends to be higher when $p_{\text{SiO,in}}$ increases, *i.e.*, at lower He/Ar gas flows. In fact, Experiments 1c, 3a, 4a and 6a have an increasing amount of nanowires produced. However, the masses of both condensation products change often between experiments from the same series. This can be attributed to the irregular profiles of the SiC particles chosen, and how they pack in the condensation chamber. In fact, nanowires production fills the void between SiC particles, and clogs the system. If the gas does not flow upwards, it will be kept in the condensation chamber.

Table II. Partial Pressures of SiO(g), Temperatures and Condensates Mass Measured in Each Setup. Reprinted with Permission and Updated from Ref. [28]

Gas Flow [l min^{-1}]	0.4	0.4	0.1	0.1	0.05	0.02	0.02	0.02	0.02	0.02	0.02	0.02
Holding Time	1 h	1 h	0.5 h	1 h	1 h	0.5 h	1 h	1 h	1 h	1 h	1 h	4 h
Experiment	1b	1c	2a	3a	4a	5a	6a	6b	6c	6d	6e	7a
$p_{\text{SiO},in}$	0.619	0.619	0.712	0.712	0.731	0.742	0.742	0.742	0.742	0.742	0.742	0.742
$p_{\text{SiO},R1,start}$	0.610	0.611	0.707	0.709	0.725	0.740	0.738	0.741	0.740	0.739	0.740	0.740
$p_{\text{SiO},out}$	0.537	0.534	0.676	0.671	0.686	0.731	0.705	0.732	0.723	0.715	0.731	0.731
$T_{\text{SiO},in}$ [$^{\circ}\text{C}$]	1815	1815	1815	1815	1815	1815	1815	1815	1815	1815	1815	1815
$T_{\text{SiO},R1,start}$ [$^{\circ}\text{C}$]	1725	1725	1725	1750	1750	1750	1750	1750	1750	1750	1750	1700
T_{out} [$^{\circ}\text{C}$]	1019	924	1247	1101	1279	1377	1268	1387	1268	1209	1427	1134
Mass of Si-SiO ₂ Condensate [g]	0.38	0.24	0.00	0.15	1.40	0.10	1.65	0.11	0.11	0.70	0.12	0.20
Mass of SiC-SiO _x Nanowires [g]	1.71	2.27	1.73	2.37	2.61	0.88	3.70	0.88	1.38	1.98	1.78	1.14

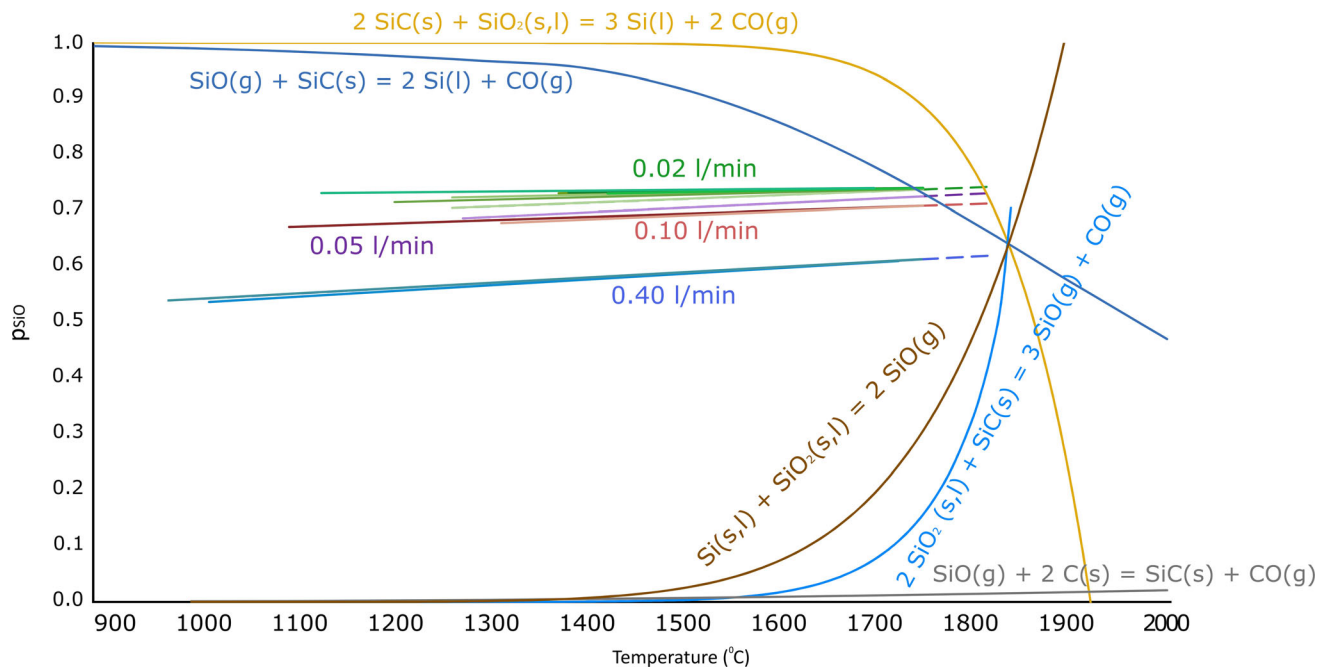


Fig. 18—Equilibrium partial pressure of SiO(g) for Reaction 3 through 7 and comparison with p_{SiO} at different inert gas flows.

Most of the nanowires are found between 1400 °C and 1600 °C.^[27] Experiments 4a and 6a became so clogged that it was necessary to destroy the graphite tube, to extract the SiC substrates from the condensation chamber.

The effect of the holding time can be seen by comparing series 5–7. Experiments lasting for shorter times will produce smaller amount of condensates. Experiments of series 6 produced more condensates than experiment 7a. Vangskåsen^[26] showed that white condensate softens and shrinks if heated above 1600 °C. This was interpreted as a back-reaction to SiO(g) and CO(g).

The composition of the gas phase in each experiment can be compared to the equilibrium composition of the gas in different reactions (Figure 18). Five curves are marked with reaction equilibria of Reactions (1, 4 through 7). In the reaction equilibria

curves, the products on the right-hand term are stable when the temperature and gas composition coordinate lies at the right-hand side (or above) of the reaction curve.

The curves confirm that all the products found in the condensation chamber are thermodynamically stable. In fact, Reaction (1) and (7) involve the condensation products. Reaction (4) is responsible for the formation of SiC on the graphite walls. Reaction (5) and (6) produced silicon in the gas production chamber walls. Vangskåsen states that elemental Si droplets are found between the nanowires. If that was the case, Si would be thermodynamically favored at temperatures below 1800 °C. However, Reaction (6) is shifted to SiO(g) and SiC where nanowires formation occurs. Si droplets were not found during nanowires characterization. The SiC particles do not interact with SiO(g) during nanowire formation.

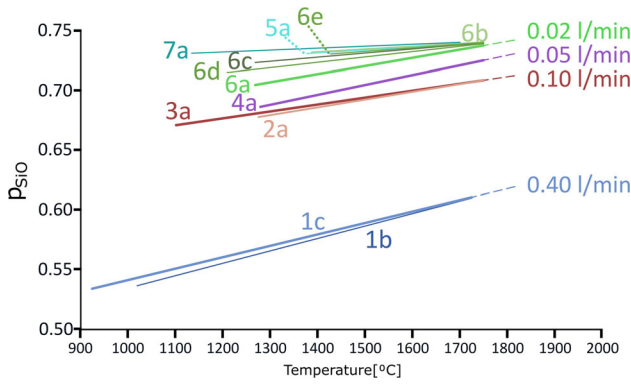


Fig. 19—Closer focus on partial pressure of SiO(g) and gas temperature in the experiments.

The straight lines in Figures 18 and 19 show the temperature and gas composition intervals in which an experiment took place. Where the line is dashed, nanowires did not form. On the other hand, Reaction (1) occurred when the line is continuous. The edges of the lines have coordinates $(T_{\text{SiO},\text{in}}; p_{\text{SiO},\text{in}})$ and $(T_{\text{SiO},\text{out}}; p_{\text{SiO},\text{out}})$. The transition between a dashed and continuous line identifies the condition $(T_{\text{SiO},\text{R1},\text{start}}; p_{\text{SiO},\text{R1},\text{start}})$.

Figure 19 shows the differences between the straight lines in the p_{SiO} range 0.50-0.75. Lines with similar colors have been collected according to the chosen He/Ar injected gas flow. The gas is still very rich in SiO(g), compared to the industrial off-gas of silicon production plants. The mass balance for the industrial off-gas calculated by Schei *et al.*^[30] estimates a p_{SiO} of 0.05. Reaction (1) and (7) together capture between 10 and 20 pct of the initial SiO(g) content. Other reactions, such as Reaction (4), may play a major role in SiO(g) capture, compared to Reactions (1) and (7).

B. Reaction Mechanism

The reaction mechanism proposed is based on the theory of the OAG mechanism by Noor Mohammad,^[25] combined with experimental results and theories from other works. Nanowire formation will take place into three steps: incubation, growth, and termination. The incubation is the seed generation step (Figure 20). The seed is the base of the nanowire, which is attached to the substrate. SiO(g) has unsaturated chemical bonds, and would rather be absorbed on the surfaces, generating more SiC seeds from chemically active sites at high temperatures.^[10] SiC and SiO_x are produced at the same time and close to each other, due to Reaction (8). For $x=2$, Reaction (1) and (8) are equal. Reaction (8) occurs on the nanowire sidewalls and the substrate surface.

The subscript x is used, since the stoichiometry of the oxide phase is uncertain at nanometric sizes. Quantitative analysis is not reliable at nanometric scale. Previous works also refer to SiO_x and not to SiO₂.^[7,8,11–15]

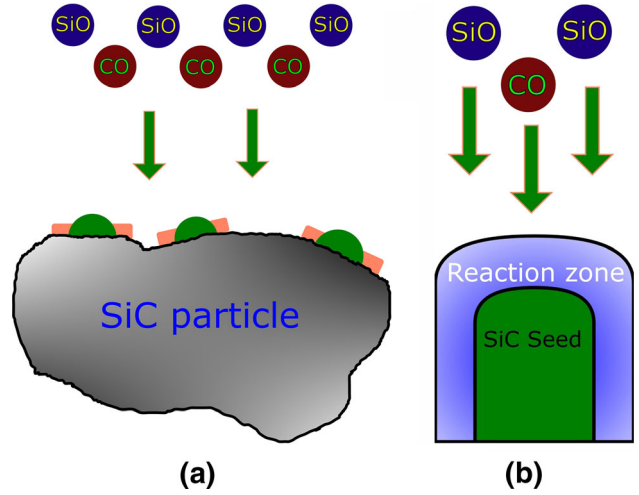
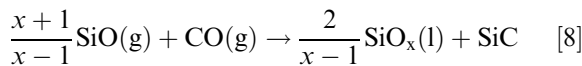
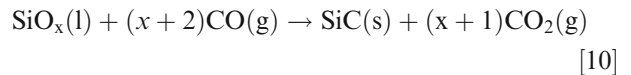
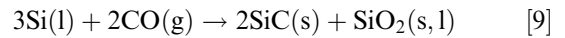


Fig. 20—Stage 1: Incubation. (a) Deposition of nanoclusters; (b) Reaction zone during incubation. Green = SiC(s); Orange: SiO_x(l).

The SiC seed grows laterally during incubation. The SiO_x external layer is generated before the vertical growth starts. SiO_x will use its dangling bonds^[34] to bind with SiC seeds sidewalls. SiO_x should prevent diffusion of the vapor species through the sidewalls, limiting the lateral growth. SiC and SiO_x will be the only species allowed to diffuse through the nanowire sidewalls. However, such species will have limited diffusion rates because of their high molecular mass.^[25]

Growth (Figure 21) starts when the lateral growth of the seed is completed, *i.e.*, once SiO_x(l) has wrapped the SiC seed. Growth continues in the preferential direction. A reaction zone will generate above the seed. The reaction zone is a liquid droplet of SiO_x(l), with solid SiC particles. The droplet is generated above the seed, and assumes the configuration seen in Figure 6. SiC and SiO_x are immiscible, as shown by the wettability tests performed by Vangskäsen.^[26] Solid SiC tends to sink at the center of the droplet and favor the vertical growth of the seed.

SiO(g) decomposes into Si(l), SiO₂(l) and SiO_x(l)^[34,35] and Reaction (8). In this area Si(l) can react with CO(g) to form SiC and SiO₂ by Reaction (9). SiO_x(l) and SiO₂(l) can react with CO(g) to generate SiC and CO₂(g) (Reactions (10) and (11))^[30] The unreacted oxides will flow and accumulate to the lateral side of the nanowire, creating SiC domains with different orientations at the sides (Figure 6). Reaction (10) is equal to Reaction (11) for $x=2$.



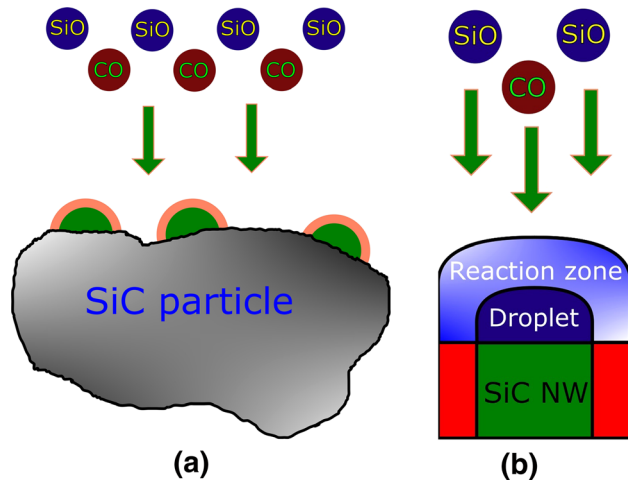


Fig. 21—Stage 2: (a) Growth; (b) Configuration of nanowires during growth. Green = SiC(s); Orange = SiO_x(l); Red = shell phase.

During growth, oxygen atoms diffuse eventually into the droplet. A small fraction of oxygen is still present after the initial crucible purging procedure. Oxygen can come from air leakages in the furnace. Crystallographic defects such as stacking faults will generate, as found during TEM analysis (Figures 6 and 7b) and as suggested by Hu *et al.*^[12]

The shell phase can be liquid, despite the melting point of SiO₂ is not reached. Nanowire production occurred between 924 °C and 1750 °C, whereas bulk silica melts at 1710 °C. TEM characterization shows that SiO_x nodules assumed a droplet shape. SiO_x can still be present in liquid state below 1710 °C for two main reasons. The first is the exothermic behavior of Reaction (1).^[28,30] The local temperature can increase above the melting point, favoring a phase transition. Reaction (1) has an enthalpy of $\Delta H^\circ = -1367.677 \text{ kJ mol}^{-1}$ at 1800 °C, as computed by the software HSC Chemistry 9[®]. The second is the melting point depression effect.^[36] It has been known for a long time that the particle size affects the melting point. Nanosized systems have lower melting points compared to the bulk system, as surface energy contributions will enter the thermodynamics of formation of new phases. Further knowledge about the evolution of the shell phase during growth is given in Broggi *et al.*^[21]

The last stage of nanowire formation is called termination. The reaction zone will be active if the SiO(g) partial pressure and temperature conditions shift Reaction (8) to its products. If these conditions are not satisfied, the growth will stop, and the droplet will solidify at the top of the nanowire. SiO_x solidifies also when the shell phase is large enough to avoid melting point depression, or when the energy freed by Reaction (8) is not heating the system locally. Figure 22 sketches the termination processes and the final configuration of the nanowire, which resembles the structure found during TEM analysis.

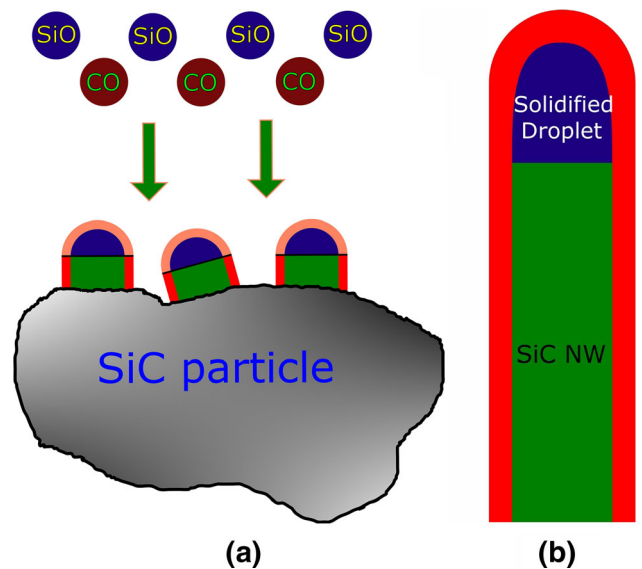


Fig. 22—Stage 3: (a) Termination; (b) Final aspect of nanowire top at terminated growth. Green = SiC(s); Orange = SiO_x(l); Red = Si + SiO₂ + SiO_x (s).

V. CONCLUSION

Core-shell SiC-SiO_x nanowires formation has been investigated by producing SiO(g) and CO(g) from a mixture of SiO₂ and SiC. The nanowires web appears as a blue (900 °C to 1250 °C; 1610 °C to 1800 °C) and white (1150 °C to 1780 °C) coating at visual inspection. When the temperature rises, the SiO_x shell phase can assume a spherical nodule shape around the SiC core phase.

A lower SiO(g) content in the gas phase will decrease the amount of SiC-SiO_x nanowires formed. When He or Ar(g) are added, nanowires form at lower temperatures and in larger temperature intervals. Temperatures will increase locally thanks to the exothermic nanowire production reaction. Melting depression effects and high local temperatures make SiO_x liquid at temperatures below the melting point of bulk silica. A two-step mechanism of reaction is proposed. First, the gas reaction will create SiO_x and SiC nanoclusters at the surface. Once the lateral growth of the nanocluster seeds is finished, the growth will continue vertically. The growth stops at low temperatures and low SiO(g) content in the gas phase.

ACKNOWLEDGMENTS

The authors would like to thank Morten Peder Raanes for the EPMA and Ingeborg-Helen Svenum (SINTEF) for the XPS analysis. The TEM work was carried out using NORTEM infrastructure, Grant 197405, TEM Gemini Centre, Norwegian University of Science and Technology (NTNU), Norway. The TEM analysis and sample preparation were done in

collaboration with Ragnhild Sæterli (NTNU). The present study was supported by Elkem AS and the EnergiX program of the Research Council of Norway through Project 269431 SiNoCO₂.

FUNDING

Open Access funding provided by NTNU Norwegian University of Science and Technology (incl St. Olavs Hospital - Trondheim University Hospital).

CONFLICT OF INTEREST Andrea Broggi, Merete Tangstad and Eli Ringdalen declare that there is no conflict of interest regarding this paper.

OPEN ACCESS

This article is licensed under a Creative Commons Attribution 4.0 International License, which permits use, sharing, adaptation, distribution and reproduction in any medium or format, as long as you give appropriate credit to the original author(s) and the source, provide a link to the Creative Commons licence, and indicate if changes were made. The images or other third party material in this article are included in the article's Creative Commons licence, unless indicated otherwise in a credit line to the material. If material is not included in the article's Creative Commons licence and your intended use is not permitted by statutory regulation or exceeds the permitted use, you will need to obtain permission directly from the copyright holder. To view a copy of this licence, visit <http://creativecommons.org/licenses/by/4.0/>.

REFERENCES

1. Y. Zhang, C.A. Pickles, and J. Cameron: *J. Reinf. Plast. Compos.*, 1992, vol. 11, pp. 1176–86.
2. A. Meng, Z. Li, J. Zhang, L. Gao, and H. Li: *J. Cryst. Growth*, 2007, vol. 308, pp. 263–68.
3. C.A. Pickles and J.M. Toguri: *J. Mater. Res.*, 1992, vol. 8, pp. 1996–2003.
4. H. Mølnås: *Project report*, Investigation of SiO-Condensate Formation in the Silicon Process, NTNU, Trondheim, Norway, 2010.
5. J. Vangskåsen: *Project report*, Investigation of the Cavity Formation in the Silicon Process, NTNU, Trondheim, Norway, 2011.
6. M.S. Khrushchev: *Inorg. Mater.*, 2000, vol. 36, pp. 462–64.
7. X.J. Wang, J.F. Tian, L.H. Bao, C. Hui, T.Z. Yang, C.M. Shen, H.-J. Gao, F. Liu, and N.S. Xu: *J. Appl. Phys.*, 2007, vol. 102, pp. 1–6.
8. S.C. Dhanalaban, M. Negri, F. Rossi, G. Attolini, M. Campanini, F. Fabbri, M. Bosi, and G. Salviati: *Mater. Sci. Forum*, 2013, vols. 740–742, pp. 494–97.
9. M. Ksiazek, I. Kero, and B. Wittgens: *Takano Int. Symp. Met. Alloys*, 2015, pp. 157–66.
10. B. Zhong, L. Kong, B. Zhang, Y. Yu, and L. Xia: *Mater. Chem. Phys.*, 2018, vol. 217, pp. 111–16.
11. P. Hu, S. Dong, K. Gui, X. Deng, X. Zhang, and R. Soc: *Chem.*, 2015, vol. 5, pp. 66403–08.
12. P. Hu, R.-Q. Pan, S. Dong, K. Jin, and X. Zhang: *Ceram. Int.*, 2016, vol. 42, pp. 3625–30.
13. H. Liu, Z. Huang, J. Huang, M. Fang, Y.-G. Liu, and X. Wu: *J. Mater. Chem. C*, 2014, vol. 2, pp. 7761–67.
14. J. Wei, K.-Z. Li, H.-J. Li, Q.-G. Fu, and L. Zhang: *Mater. Chem. Phys.*, 2006, vol. 95, pp. 140–44.
15. R. Wu, B. Zha, L. Wang, K. Zhou, and Y. Pan: *Phys. Status Solidi A*, 2012, vol. 209, pp. 553–58.
16. J.-S. Lee, Y.-K. Byeun, S.-H. Lee, and S.-C. Choi: *J. Alloys Compd.*, 2008, vol. 456, pp. 257–63.
17. P. Kang, B. Zhang, G. Wu, and H. Gou: *Mater. Lett.*, 2011, vol. 2011 (65), pp. 3461–64.
18. H. Huang, J.T. Fox, F.S. Cannon, and S. Komarneni: *Ceram. Int.*, 2011, vol. 37, pp. 1063–72.
19. G.W. Meng, L.D. Zhang, C.M. Mo, S.Y. Zhang, H.J. Li, Y. Qin, and S.P. Feng: *Metall. Mater. Trans. A*, 1999, vol. 30A, pp. 213–19.
20. M. Saito, S. Nagashima, and A. Kato: *J. Mater. Sci. Lett.*, 1992, vol. 11, pp. 373–76.
21. A. Broggi, E. Ringdalen, and M. Tangstad: *presented at Int. Conf. Silicon Carbide Relat. Mater.*, Kyoto (Japan), 2019.
22. W.E.Jr. Hollar and J. Kim, in: *Proc. 15th Annu. Conf. Compos. Adv. Ceram. Mater.*, Wiley, Hoboken, NJ, 1991.
23. X. Li, G. Zhang, R. Tronstad, and O. Ostrovski: *Ceram. Int.*, 2016, vol. 42, pp. 5668–5676.
24. R.-Q. Zhang, Y. Lifshitz, and S.-T. Lee: *Adv. Mater.*, 2003, vol. 15, pp. 635–640.
25. S. Noor Mohammad, *J. Vac. Sci. Technol. B* 2008, 26, 1993–2007.
26. J. Vangskåsen, *Metal-Producing Reactions in the Carbothermic Silicon Process*, Master thesis, NTNU, Department of Materials Science and Engineering, 2012.
27. A. Broggi, M. Tangstad, and E. Ringdalen: *Silicon for the Chemical and Solar Industry XIV*, Svolvær, Norway, 2018, pp. 139–152.
28. A. Broggi, M. Tangstad, and E. Ringdalen: *Metall. Mater. Trans. B*, 2019, vol. 50B, pp. 2667–2680.
29. E. Myrhaug, *Non Fossil Reduction Materials in the Silicon Process-Properties and Behaviour*, Doctoral thesis, NTNU, Department of Materials Science and Engineering, 2003.
30. A. Schei, J. Tuset, and H. Tveit: *Production of High Silicon Alloys*, 1st ed., Tapir, Trondheim, 1998.
31. V. Andersen, *Reaction Mechanism and Kinetics of the High Temperature Reactions in the Silicon Process*, Master thesis, NTNU, Department of Materials Science and Engineering, 2010.
32. M. Tangstad, J. Safarian, S. Bao, E. Ringdalen, and A. Valderhaug: *Asp. Min. Miner. Sci.*, 2019, vol. 3, pp. 1–11.
33. A. Broggi, *Condensation of SiO(g) and CO(g) in silicon production*, Doctoral thesis, NTNU, Department of Materials Science and Engineering, 2021 (to be published).
34. K. Schulmeister, W. Mader, and J. Non-Cryst: *Solids*, 2003, vol. 320, pp. 143–50.
35. A. Hohl, T. Wieder, P.A. Van Aken, T.E. Weirich, G. Denninger, M. Vidal, S. Oswald, C. Deneke, J. Mayer, H. Fuess, and J. Non-Cryst: *Solids*, 2003, vol. 320, pp. 255–80.
36. S. Stølen and T. Grande: *Chemical Thermodynamics of Materials: Macroscopic and Microscopic Aspects*, 1st ed., Wiley, New York, 2004.

Publisher's Note Springer Nature remains neutral with regard to jurisdictional claims in published maps and institutional affiliations.